International Journal of Environmental Research and Public Health

MDPI

*Article*

# A Soil Moisture Prediction Model Based on Depth and Water Balance Equation: A Case Study of Xilingol League Grassland

**Rong Fu [1], Luze Xie[1], Tao Liu [2*], Binbin Zheng[1], Yibo Zhang[1], Shuai Hu[3]**

[1] The College of Economics, Hangzhou Dianzi University, Hangzhou, 310018, China; E-mails: furong@hdu.edu.cn (R.F.); 211150030@hdu.edu.cn (L.X.); 212150051@hdu.edu.cn (B.Z.); 212150079@hdu.edu.cn (Y.Z.)
[2] Department of Sociology, Hangzhou Dianzi University, Hangzhou, 310018, China; E-mails: liutao@hdu.edu.cn (T.L.)
[3] College of Computer Science and Technology, Hangzhou Dianzi University, Hangzhou, 310018, China; E-mails: hshs@hdu.edu.cn (S.H.)
* Correspondence: liutao@hdu.edu.cn (T.L.)

**Abstract:** Soil moisture plays an important role in ecology, hydrology, agriculture and climate change. This study proposes a soil moisture prediction model based on depth and water balance equation, which integrates the water balance equation with the seasonal ARIMA model, and introduces the depth parameter to consider the soil moisture at different depths. The experimental results showed that the model proposed in this study was able to provide higher prediction accuracy for soil moisture at 40 cm, 100 cm and 200 cm depths compared to the seasonal ARIMA model. Different models were used for different depths, in this study, the seasonal ARIMA model was used at 10 cm, and the proposed model was used at 40 cm, 100 cm and 200 cm, from which more accurate prediction values could be obtained. The fluctuation of the predicted data has a certain seasonal trend, but the regularity decreases with increasing depth until the soil moisture is almost independent of external influence at 200 cm depth. Accurate prediction of soil moisture can contribute to the scientific management of grasslands, thus promoting ecological stability and sustainable development of grasslands while rationalizing land use.

**Keywords:** soil moisture prediction; water balance equation; seasonal ARIMA model; sustainable development; land use

**Citation:** To be added by editorial staff during production.

Academic Editor: Firstname Lastname

Received: date
Accepted: date
Published: date

**Publisher's Note:** MDPI stays neutral with regard to jurisdictional claims in published maps and institutional affiliations.

**Copyright:** © 2022 by the authors. Submitted for possible open access publication under the terms and conditions of the Creative Commons Attribution (CC BY) license (https://creativecommons.org/licenses/by/4.0/).

## 1. Introduction

As a natural ecohydrological resource, soil moisture (SM) is an important aspect of the heat transfer process and energy exchange between the surface and atmospheric system, as well as the key link of the surface and groundwater circulation and the land carbon cycle[1]. It plays an important role in many aspects. In the ecological field, changes in soil moisture are associated with changes in vegetation cover and have a significant impact on forest decline, land degradation and loss of biodiversity[2]. In the field of hydrology, soil moisture is an important indicator to assess the degree of drought, and different soil moisture levels can bring about deviations in physical patterns[3]. In agriculture, on the one hand, soil moisture affects the length of the grazing season, the growth rate of grasses and nutrient uptake; too much soil moisture affects crop root respiration and too little soil moisture limits crop uptake of fertilizers[4]. On the other hand, it limits the dissolution and transfer of nutrients and microbial activity in the soil[5], leading to nutrient loss to the wider environment and thus affecting crop yields. In the climate domain, soil moisture limits transpiration and photosynthesis of plants, which in turn has an impact on water, energy and biogeochemical cycles, while persistence of soil moisture leads to persistence of the climate system. Conversely, changes in climate also have an impact on soil moisture, creating a soil moisture-climate interaction[6]. Therefore, soil moisture is of critical importance in ecology[7], hydrology[8], agriculture[9] and climate change[10,11]

research, and accurate prediction of soil moisture can provide important guidance for drought prevention, grazing irrigation and other scientific applications[12].

Soil moisture is influenced by a variety of factors such as precipitation[13], evaporation[14], soil properties[15], and vegetation[16], and the predictability of soil moisture may result from its own persistence or from external forcing factors[17]. Thus, soil moisture prediction not only exhibits a degree of uncertainty, but also the highly nonlinear variation relationship between explanatory variables and soil moisture makes its prediction very difficult. Prediction methods for soil moisture fall into two main categories: physics-based process models and data-driven empirical models. Physics-based process models focus on hydrological processes that control soil moisture transfer mechanisms through physical equations and calculate explanatory variables as part of land surface data assimilation techniques. Factors such as precipitation, atmospheric temperature, and solar radiation, driven by model-generated or observationally obtained factors, can be used for seasonal flow prediction, such as soil moisture, runoff and so on[18]. For example, Huang explored the dynamics of soil moisture in the Weihe River basin through water balance equations[19]; Tang used a two-parameter monthly water balance model to predict runoff[20]. However, the physical model is complicated, and the absence or lack of information may bring some errors to soil moisture prediction. Furthermore, because the equations are based on the assumption of independence of local laws, they are not applicable to medium- and long-term predictions. Data-driven empirical models are based mainly on constructing mappings of explanatory variables and soil moisture. The widely used statistical methods include multiple linear regression models[21,22], Bayesian models[23], and support vector machine models[24,25]. For example, using time series[26] and multiple regression analysis methods[27] in statistical methods, forecasting is achieved by establishing autocorrelation of historical soil moisture and multiple regression equations between the explanatory variables and soil moisture. Currently, many artificial intelligence methods and techniques also exist for soil moisture prediction[28,29], and the material sources are mainly satellite remote sensing data, satellite images, and microwave radar data[30]. Satellite remote sensing imaging, although intuitive, is often only applicable to the exploration and monitoring of materials visible on the surface. For example, remote sensing techniques can only effectively invert the moisture content of the soil surface, and vegetation can be another major cause of information loss, in addition to the winter snow and ice cover that can impact information utilization. Moreover, deep learning models are questionable due to the inaccessibility of the theoretical rationale for their predictions.

In order to accurately predict soil moisture at different depths in Xilingol League grassland of Inner Mongolia, and then provide reference for the research of grazing ecology theory and sustainable grassland utilization practice, a soil moisture prediction model based on depth and water balance equation is proposed to address the shortcomings of the physical-based process model and the data-driven empirical model. The model combines a water balance equation and the seasonal ARIMA model. The model predicts soil moisture at 10 cm, 40 cm, 100 cm and 200 cm in the test plots by considering the effect of depth variation on soil moisture and thus introducing a depth parameter $\gamma$. The model has high prediction accuracy in predicting soil moisture at 40 cm, 100 cm and 200 cm. Different models were used for different depths, in this study, the seasonal ARIMA model at 10 cm and the proposed model at 40 cm, 100 cm and 200 cm, which resulted in more accurate prediction values and provided an important reference for developing appropriate irrigation and grazing plans and water management, as well as improving drought prediction and agricultural crop yields.

The rest of the paper is organized as follows: Section 2 presents the data and model methodology used in this study. Section 3 empirically analyzes the soil moisture predictions and compares the model predictions. Section 4 discusses the theoretical contributions, policy implications, limitations and future research perspectives of the study. The overall empirical procedure is shown in the Figure 1 below.

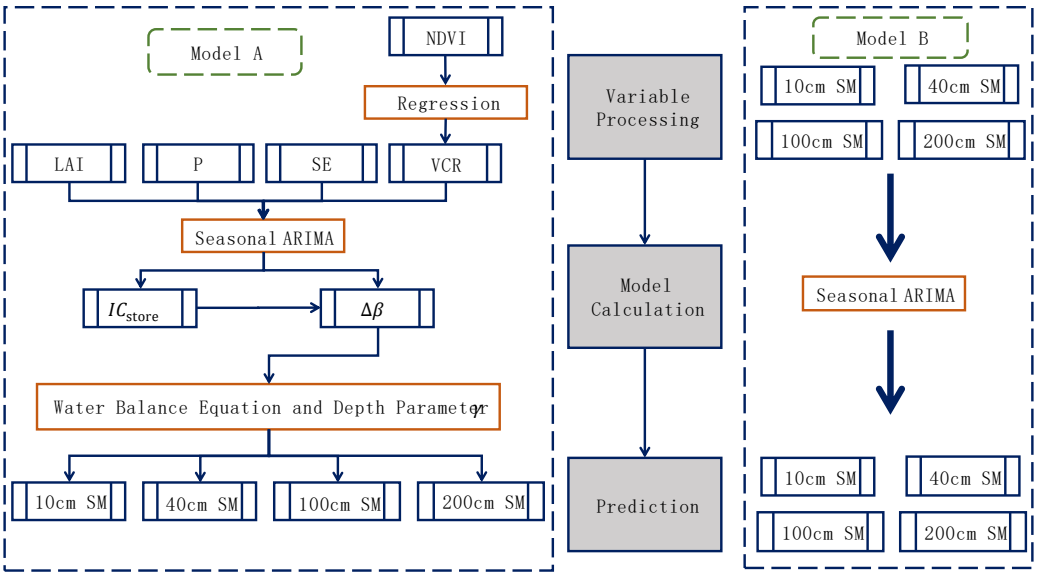



**Figure 1.** Empirical flow chart of soil moisture prediction model.

## 2. Materials and Methods

### *2.1. Study Area and Data Acquisition*

The Xilingol League Grassland in Inner Mongolia is located on the Xilin River in the Inner Mongolia Plateau, with geographical coordinates between 110°50′~119°58′ E and 41°30′~46°45′ N. The total area of Xilingol League Grassland is 19.2 million hectares, and the grassland landscape is a high plain with elevation between 800-1200 meters. In the climate zone, the Xilin River basin belongs to the temperate subarid region, and its climate type belongs to the temperate semi-arid grassland climate in the continental climate. The four seasons are distinct: spring is often accompanied by windy weather, summer is warm and humid, while autumn and winter are cold and dry. According to the meteorological monitoring data of Inner Mongolia grassland station, the annual sunshine hours in the area is 2603.8h, the average annual temperature is 0.96℃, the average annual evaporation is 1664.6mm/year, the average rainfall is about 340mm, and the inter-month variation of precipitation is large, mainly concentrated in June-September, accounting for about 74.4% of the annual precipitation. The topographic soil type is mainly chestnut-calcium soil, and the plant community is most widely distributed by sheep grass (Leymus chinensis) community and big needle grass (Stipa grandis) community. Inner Mongolia Xilingol League grassland is not only an important national livestock production base, but also an important green ecological barrier that plays a role in reducing the occurrence of dust storms and severe weather. It is also one of the typical areas for studying ecosystem response mechanisms to human disturbance and global climate change and an important part of the terrestrial sample belt in the International Geosphere-Biosphere Program (IGBP) - Northeast China Terrestrial Ecosystem Sample Belt (NECT). Therefore, the accurate prediction of soil moisture has a positive impact on the sustainable development of grasslands.

The observation points for this study were 115°22.5′ E, 44°7.5′ N. The variables used were precipitation (P), soil evaporation (SE), normalized difference vegetation index (NDVI), vegetation coverage rate (VCR), soil depth, and leaf area index (LAI). Data were obtained from the National Glacial Tundra Desert Science Data Center (http://www.ncdc.ac.cn/portal/metadata/), the U.S. Geological Survey (https://ladsweb.modaps.eosdis.nasa.gov/search/), the Ecology Discipline Data Center of the Chinese Academy of Sciences (http://www.nesdc.org.cn/sdo/detail?id=609de9c07e28176b33e8743d), and the wheatA small malt-agrometeorological big data system (v1.5.1) software. The information of each variable is summarized in Table 1.

**Table 1.** Observed values of each variable.

| Variables | Longitude | Latitude | Starting time | End time | Unit | Length |
|---|---|---|---|---|---|---|
| LAI | | | | | m2/m2 | 123 |
| NDVI | | | | | — | 123 |
| SE | | | | | mm | 123 |
| P | | | | | mm | 123 |
| 10cm SM | 115.375 | 44.125 | 2012.1 | 2022.3 | kg/m2 | 123 |
| 40cm SM | | | | | kg/m2 | 123 |
| 100cm SM | | | | | kg/m2 | 123 |
| 200cm SM | | | | | kg/m2 | 123 |
| VCR | | | 2020.7 | | % | 21 |

### *2.2. Methods*

#### 2.2.1. A Soil Moisture Prediction Model Based on Depth and Water Balance Equation

The water cycle in grassland is cyclic, with water vapor transport through precipitation, infiltration and evaporation. The water balance equation of the soil-vegetation-atmosphere system without considering anthropogenic factors is

$$\Delta\beta_t = \beta_t - \beta_{t-1} = P_t + G_{u,t} + R_{in,t} - \left(Et_{a,t} + G_{d,t} + R_{out,t} + IC_{store,t}\right) \quad (1)$$

In equation (1), $\beta_t$ is the soil moisture in period t and $\Delta\beta$ is the variation of soil moisture. At time t, $P_t$ is precipitation, $G_{u,t}$ and $G_{d,t}$ are groudwater capillary rise and soil water infiltration. $Et_{a,t}$ is soil evaporation, which is expressed by SE in this study. $R_{in,t}$ and $R_{out,t}$ are inlet and outlet runoff, and $IC_{store,t}$ is the vegetation interception flow.

The grassland of Xilingol League is located in the plain area, the terrain is flat, the precipitation distribution is unstable, the intensity of precipitation is generally low, the water circulation is mainly vertical exchange, the inlet and outlet runoff of the whole grassland can be regarded as roughly equal, so for the simplification of the model we assume that $R_{in,t} - R_{out,t} = 0$. Since the data of groundwater resource circulation are not available, the groundwater and soil contact, the exchange water resources can also be assumed to be roughly equal, which means that $G_{u,t} - G_{d,t} = 0$. Therefore, the amount of soil moisture change is mainly related to precipitation, evaporation and vegetation interception flow.

Vegetation interception flow is a variable that is mainly related to precipitation, vegetation coverage rate and leaf area index[31,32]. The vegetation interception flow is negatively correlated with precipitation and positively correlated with vegetation cover and leaf area index, which means that the lower the precipitation, the higher the vegetation cover and the higher the leaf area index, the higher the vegetation interception flow. It can be expressed as

$$IC_{store,t} = c_{p,t} \times IC_{max} \times \left(1 - e^{\frac{-k \times R_{cum,t}}{IC_{max}}}\right) \quad (2)$$

In equation (2), $c_{p,t}$ denotes the vegetation coverage rate in period t, which is represented by VCR in this study; $k$ is the correction factor for vegetation density, which is related to the leaf area index; $R_{cum,t}$ is the accumulated precipitation, and in this study the precipitation from period t-1 to period t is equivalent to $P_t$. $IC_{max}$ is the maximum interception of the particular vegetation, which can be estimated by the LAI[33], whose expression is

$$IC_{max} = 0.935 + 0.498 \times LAI - 0.00575 \times LAI^2 \quad (3)$$

Since LAI, P, SE and VCR are all time series, they are greatly influenced by seasonal environment. Therefore, the seasonal ARIMA model is used for prediction, and the specific steps are as follows.

1. Determine the stationary of the series. Testing the stationarity of the series with unit root test. If the series is non-stationary, it needs to be differenced to eliminate the series fluctuations to make the data stationary, and extract the effective information in the series.
2. Model order determination. The optimal order is firstly determined by the trailing and truncation of ACF and PACF, and then the final parameters are determined by trial-and-error method based on AIC in the range around the initially determined parameters.
3. Model testing. The white noise test on the residuals of the model. If there are insignificant parameters, they need to be removed and the model structure is readjusted. The white noise test ensures that the model can fully extract the relevant information of the series.

As a result, we obtain the prediction model as: $\beta_{t+1} = \beta_t + \Delta\beta$. Considering the effect of depth h variation on soil moisture, the depth parameter $\gamma$ is introduced, and finally the soil moisture prediction model based on depth and water balance equation is obtained as follows.

$$\beta_{\mathrm{h,t+1}} = \beta_{h,t} + \gamma \times \Delta\beta = \beta_{h,t} + \gamma_h \times \left[P_t - \left(SE_{\mathrm{t}} + IC_{store,t}\right)\right] \quad (4)$$

2.2.2. A Soil Moisture Prediction Model Based on Seasonal ARIMA Model

Soil moisture is a time series that varies with month when only its own variation is considered, and has certain seasonal characteristics. The univariate prediction of soil moisture is thus validated for comparison using a seasonal ARIMA model.

In practice, the stationary process and parameter adjustment process for the time series is very time consuming. It is necessary to keep the data stationary when constructing ARMA or ARIMA models, and the process of determining the p and q values is tedious and not easy to reach the exact values. The auto.arima function can eliminate the process of determining p and q values and make the model more acceptable to the data[34]. Therefore, this study uses the auto.arima function to determine each parameter.

The seasonal ARIMA (p, d, q) ($P_S$, $D_S$, $Q_S$) model is based on the ARIMA (p, d, q) model and is used to deal with series where there is a significant periodicity due to seasonal variations. The seasonal ARIMA model automatically determines the d, p and q values through the auto.arima function and fits the model on a univariate series, from which soil moisture inputs at different depths can be predicted.

2.2.3. Error Estimation

For the purpose of assessing the validity and accuracy of the model, this study uses MSE (Mean Squared Error), RMSE (Root Mean Squared Error), MAE (Mean Absolute Error) and MAPE (Mean Absolute Percentage Error) to evaluate the model.

$$MSE = \frac{1}{n}\sum_{i=1}^{n}(\hat{y}_i - y_i)^2 \quad (5)$$

$$RMSE = \sqrt{\frac{1}{n}\sum_{i=1}^{n}(\hat{y}_i - y_i)^2} \quad (6)$$

$$MAE = \frac{1}{n}\sum_{i=1}^{n}|\hat{y}_i - y_i| \quad (7)$$

$$MAPE = \frac{100}{n}\sum_{i=1}^{n}\left|\frac{\hat{y}_i - y_i}{y_i}\right| \quad (8)$$

In the above equation n is the total number of test sets, $\hat{y}_i$ is the predicted value, and $y_i$ is the actual value.

## 3. Results and Discussion

### *3.1. Model Construction and Prediction*

#### 3.1.1. The Soil Moisture Prediction Model Based on Depth and Water Balance Equation

To begin with, this study conducted descriptive statistical analysis of the variables involved, as shown in Table 2. The main independent variables involved were soil evaporation (SE), precipitation (P) and normalized difference vegetation index (NDVI). Among them, the variance of P is large, with a range of 891.79, which means that there is a large amount of precipitation in the rainy season and no precipitation for a month in the dry season, and precipitation fluctuates. The variance of NDVI is small, and the minimum value -0.02 means that the ground cover is highly reflective of visible light such as water and snow, and the overall rate of change is small. The fluctuation of SE is in between.

**Table 2.** Descriptive statistics of P, NDVI, and SE.

| Independent variable | N | Range | Minimum | Maximum | Mean | Standard Deviation |
|---|---|---|---|---|---|---|
| P | 123 | 891.79 | 0 | 891.79 | 80.83 | 143.07 |
| NDVI | 123 | 0.62 | -0.02 | 0.61 | 0.24 | 0.15 |
| SE | 123 | 38.99 | 0.27 | 39.26 | 9.87 | 9.75 |

The dependent variable to be studied is the soil moisture at different depths, and the descriptive statistics table of known data is shown below in Table 3. The coefficient of variation of soil moisture at different depths can be clearly calculated from the table: 100cm > 10cm > 40cm > 200cm. The reason for the large change in soil moisture of 10cm may be close to the surface, which is strongly affected by factors such as surface evaporation and precipitation, and any of these factors will lead to changes in soil moisture, which will fluctuate back and forth in an interval. The reason for the small variation in soil moisture of 40cm may be that it is less affected by the surface and surface water infiltration. The largest variation in soil moisture of 100cm may be due to the large influence of surface water infiltration, and the large difference in humidity between the dry season and the rainy season, resulting in large fluctuations. The minimal variation in soil moisture at 200 cm may be due to the fact that deep underground, the effect of factors such as evaporation from the surface is negligible.

**Table 3.** Descriptive statistics of soil moisture data at different depths.

| Dependent variable | Range | Minimum | Maximum | Mean | Standard Deviation | Coefficient of Variation |
|---|---|---|---|---|---|---|
| 10cm SM | 12.46 | 9.64 | 22.1 | 14.57 | 2.85 | 0.20 |
| 40cm SM | 31.99 | 29.71 | 61.7 | 42.38 | 7.48 | 0.18 |
| 100cm SM | 51.09 | 42.36 | 93.45 | 55.35 | 14.54 | 0.26 |
| 200cm SM | 4.08 | 164.48 | 168.56 | 167.22 | 0.98 | 0.01 |

In order to visualize the variation of soil moisture at different depths, a line graph was drawn as shown in Figure 2. It is also clear from this graph that the soil moisture at 200 cm is almost a straight line with small variations. The soil moisture of 10 cm fluctuates back and forth within a small interval. The variation in soil moisture was greater at 40 cm and 100 cm and was similar for both.

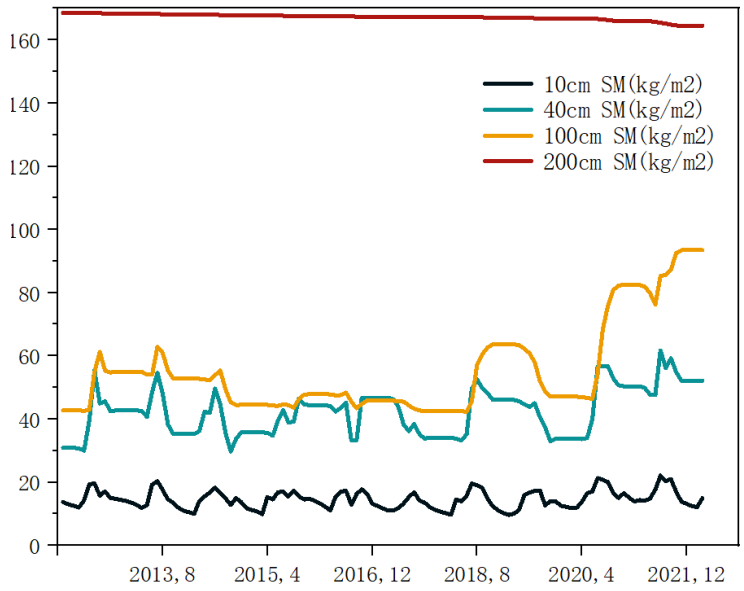



**Figure 2.** Line graph of historical soil moisture data at different depths.

According to the soil moisture prediction model based on depth and water balance equation constructed above, the data of VCR are needed to be obtained. However, the VCR has only partial data from August 2020 to 2022, and the data are relatively few. There is a close relationship between NDVI and VCR[35], so this study uses a regression model to construct a model of NDVI and VCR. Then the VCR from 2012 to July 2020 was obtained by substituting the known NDVI from 2012 to July 2020 into the regression equation.

In order to investigate which model is more suitable for fitting NDVI and VCR, linear regression, quadratic regression and cubic regression were constructed in the text, and the model summary is listed in Table 4. It shows that the F-test of linear, quadratic and cubic regressions are significant. Since the adjusted R-squared of the cubic regression is the largest and all the coefficients in the cubic regression is significant at the 0.05 level, the method used in this paper is the cubic regression.

**Table 4.** Analysis of different regression fitting results.

| model | Models Summary | | Parameter Estimates | | | |
|---|---|---|---|---|---|---|
| | Adjust R-squared | Prob(F-test) | c | b1 | b2 | b3 |
| linear | 0.764 | 0.000 | -0.055* | 0.607*** | | |
| quadratic | 0.826 | 0.000 | -0.011 | 0.067 | 0.941** | |
| cubic | 0.864 | 0.000 | 0.008 | -0.894* | 5.827** | -5.778* |

*Note: "*" means significant at 0.05; "**" means significant at 0.01; "***" means significant at 0.001.

The regression equation for NDVI and VCR can be obtained from the parameter estimates in Table 4 as

$$\widehat{\mathrm{VCR}} = 0.008 - 0.894NDVI + 5.827NDVI^2 - 5.778NDVI^3 \quad (9)$$

The resulting fitted VCR data values for 2012 to July 2020 is shown in Table 5.

**Table 5.** Fitted VCR data values for 2012 to July 2020.

| Time | 2012 | 2013 | 2014 | 2015 | 2016 | 2017 | 2018 | 2019 | 2020 |
|---|---|---|---|---|---|---|---|---|---|
| Jan | 0.006 | 0.006 | 0.000 | 0.000 | 0.024 | 0.000 | 0.000 | 0.018 | 0.016 |
| Feb | 0.006 | 0.013 | 0.006 | 0.000 | 0.024 | 0.000 | 0.004 | 0.018 | 0.006 |
| Mar | 0.000 | 0.009 | 0.002 | 0.000 | 0.000 | 0.000 | 0.000 | 0.012 | 0.006 |

| | | | | | | | | | |
|---|---|---|---|---|---|---|---|---|---|
| Apr | 0.000 | 0.004 | 0.004 | 0.000 | 0.000 | 0.000 | 0.002 | 0.004 | 0.000 |
| May | 0.012 | 0.034 | 0.044 | 0.031 | 0.015 | 0.002 | 0.009 | 0.021 | 0.006 |
| Jun | 0.220 | 0.278 | 0.138 | 0.188 | 0.077 | 0.018 | 0.021 | 0.073 | 0.066 |
| Jul | 0.310 | 0.216 | 0.246 | 0.275 | 0.160 | 0.110 | 0.321 | 0.138 | |
| Aug | 0.321 | 0.266 | 0.181 | 0.249 | 0.168 | 0.192 | 0.322 | 0.134 | |
| Sep | 0.278 | 0.196 | 0.151 | 0.181 | 0.126 | 0.106 | 0.281 | 0.089 | |
| Oct | 0.089 | 0.073 | 0.062 | 0.062 | 0.051 | 0.041 | 0.097 | 0.037 | |
| Nov | 0.000 | 0.037 | 0.024 | 0.018 | 0.018 | 0.024 | 0.037 | 0.012 | |
| Dec | 0.000 | 0.024 | 0.018 | 0.000 | 0.015 | 0.000 | 0.018 | 0.002 | |

After completing the data on VCR, the line graphs of SE, P, LAI, and VCR were plotted in Figure 3, from which it was clear that there was a direct and significant seasonal trend in these four variables. From this, the seasonal ARIMA model can be used to estimate the prediction of the time series.

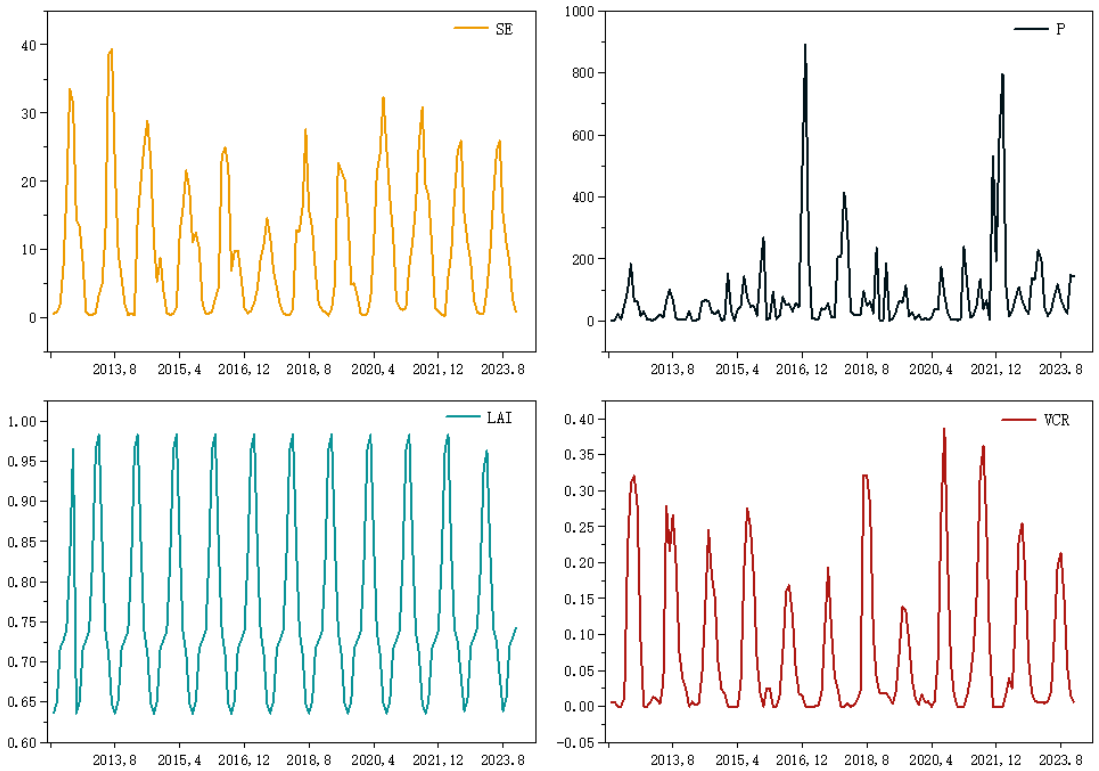



**Figure 3.** Historical data of SE, P and LAI and fitted VCR data.

The predicted data of SE, P, LAI and VCR by the seasonal ARIMA model are shown in Table 6. From the predicted data and model calculations, $IC_{max} = 1.419$. To simplify the model, we assume that the vegetation density has little effect, so the value of k is set to 1 by default in this study. $IC_{store}$ and $\Delta\beta$ can be calculated by substituting the data, both of which are also shown in Table 7.

**Table 6.** Prediction data for SE, P, LAI and VCR, and the fitted values of $\boldsymbol{IC_{store}}$ and $\boldsymbol{\Delta\beta}$.

| Year | Month | SE | P | LAI | VCR | $\boldsymbol{IC_{store}}$ | $\boldsymbol{\Delta\beta}$ |
|---|---|---|---|---|---|---|---|
| 2022 | 4 | 9.296 | 14.264 | 0.838 | 0.039 | 0.055 | -8.875 |
| | 5 | 17.656 | 33.754 | 0.741 | 0.025 | 0.036 | -16.567 |
| | 6 | 24.471 | 74.185 | 0.725 | 0.122 | 0.173 | -22.171 |
| | 7 | 25.942 | 108.964 | 0.682 | 0.233 | 0.331 | -22.64 |

| | | | | | | | |
|---|---|---|---|---|---|---|---|
| | 8 | 15.124 | 67.196 | 0.639 | 0.254 | 0.361 | -13.245 |
| | 9 | 11.049 | 39.607 | 0.654 | 0.183 | 0.26 | -9.989 |
| | 10 | 8.091 | 22.844 | 0.72 | 0.065 | 0.092 | -7.422 |
| | 11 | 2.577 | 136.693 | 0.73 | 0.018 | 0.026 | 1.953 |
| | 12 | 0.85 | 132.998 | 0.742 | 0.008 | 0.011 | 3.573 |
| | 1 | 0.599 | 228.851 | 0.813 | 0.005 | 0.007 | 7.022 |
| | 2 | 0.708 | 192.757 | 0.94 | 0.006 | 0.008 | 5.709 |
| | 3 | 4.077 | 44.006 | 0.963 | 0.004 | 0.006 | -2.617 |
| | 4 | 9.304 | 15.334 | 0.839 | 0.007 | 0.01 | -8.803 |
| | 5 | 17.672 | 36.285 | 0.742 | 0.021 | 0.03 | -16.493 |
| 2023 | 6 | 24.493 | 79.747 | 0.725 | 0.102 | 0.145 | -21.98 |
| | 7 | 25.966 | 117.134 | 0.683 | 0.196 | 0.278 | -22.339 |
| | 8 | 15.138 | 72.234 | 0.639 | 0.214 | 0.303 | -13.033 |
| | 9 | 11.059 | 42.577 | 0.654 | 0.154 | 0.218 | -9.858 |
| | 10 | 8.099 | 24.557 | 0.72 | 0.055 | 0.077 | -7.358 |
| | 11 | 2.58 | 146.942 | 0.73 | 0.015 | 0.022 | 2.297 |
| | 12 | 0.851 | 142.97 | 0.742 | 0.006 | 0.009 | 3.906 |

Since $IC_{store}$ is directly related to P and VCR, $IC_{store}$ is 0 when there is no rainfall in dry season and no vegetation covered by snow and ice in winter. According to the model constructed above, the soil moisture $\beta_{h,t+1}$ at depth h of the nth+1st month can be calculated by the soil moisture variation $\Delta\beta$, the depth coefficient $\gamma$ and the soil moisture $\beta_{h,t}$ of the nth month. The depth coefficient $\gamma$ is continuously fitted according to different depths and finally the specific values are obtained as shown in Table 7. The resulting soil moisture prediction data are also shown in Table 7.

**Table 7.** Predicted values of soil moisture based on water balance equation and seasonal ARIMA model.

| Year | Month | 10cm SM $\gamma_{10} = 0.01$ | 40cm SM $\gamma_{40} = 0.08$ | 100cm SM $\gamma_{100} = -0.15$ | 200cm SM $\gamma_{200} = 0.01$ |
|---|---|---|---|---|---|
| | 4 | 14.85 | 51.26 | 95.07 | 164.37 |
| | 5 | 14.69 | 49.96 | 97.50 | 164.21 |
| | 6 | 14.48 | 48.31 | 100.60 | 164.00 |
| | 7 | 14.24 | 46.36 | 104.26 | 163.76 |
| 2022 | 8 | 14.08 | 45.12 | 106.59 | 163.60 |
| | 9 | 13.98 | 44.27 | 108.18 | 163.50 |
| | 10 | 13.91 | 43.73 | 109.19 | 163.43 |
| | 11 | 13.96 | 44.15 | 108.39 | 163.48 |
| | 12 | 14.00 | 44.41 | 107.91 | 163.52 |
| | 1 | 14.07 | 45.05 | 106.72 | 163.59 |
| | 2 | 14.17 | 45.77 | 105.36 | 163.69 |
| | 3 | 14.15 | 45.64 | 105.61 | 163.67 |
| | 4 | 14.07 | 45.00 | 106.81 | 163.59 |
| | 5 | 13.92 | 43.77 | 109.11 | 163.44 |
| | 6 | 13.71 | 42.14 | 112.18 | 163.23 |
| 2023 | 7 | 13.46 | 40.17 | 115.87 | 162.98 |
| | 8 | 13.31 | 38.96 | 118.14 | 162.83 |
| | 9 | 13.21 | 38.10 | 119.74 | 162.73 |
| | 10 | 13.15 | 37.61 | 120.66 | 162.67 |
| | 11 | 13.15 | 37.65 | 120.60 | 162.67 |
| | 12 | 13.17 | 37.79 | 120.33 | 162.69 |

3.1.2. The Soil Moisture Prediction Model Based on Seasonal ARIMA Model

In order to compare the accuracy of the predictions, a soil moisture prediction model based on seasonal ARIMA model was constructed in this study. The auto.arima function is used to select the model with the smallest AIC and BIC, and the constructed 10cm, 40cm, 100cm and 200cm models are shown in equations (10) to (14).

$$\nabla_{12}\widehat{\beta_{10,t}} = \frac{(1-0.7593B^{12})}{(1-0.5852B)}\varepsilon_t \tag{10}$$

$$\nabla\widehat{\beta_{40,t}} = \frac{(1-0.9869B)}{(1-1.0677B+0.2250B^2)(1-0.4081B^{12}-0.2313B^{24})}\varepsilon_t \tag{11}$$

$$\nabla\widehat{\beta_{100,t}} = (1+0.5308\mathrm{B})\varepsilon_t \tag{12}$$

$$\nabla^2\widehat{\beta_{200,t}} = \frac{(1-0.9237\mathrm{B}-0.6746B^2+0.8232B^3)(1-0.3649B^{12}+0.4964B^{24})}{(1-0.7436B-0.59230B^2+0.8941B^3)(1-0.6271B^{12})}\varepsilon_t \tag{13}$$

Meanwhile, QQ plots of the fitted models with the residuals are plotted separately, as shown in Figure 4.

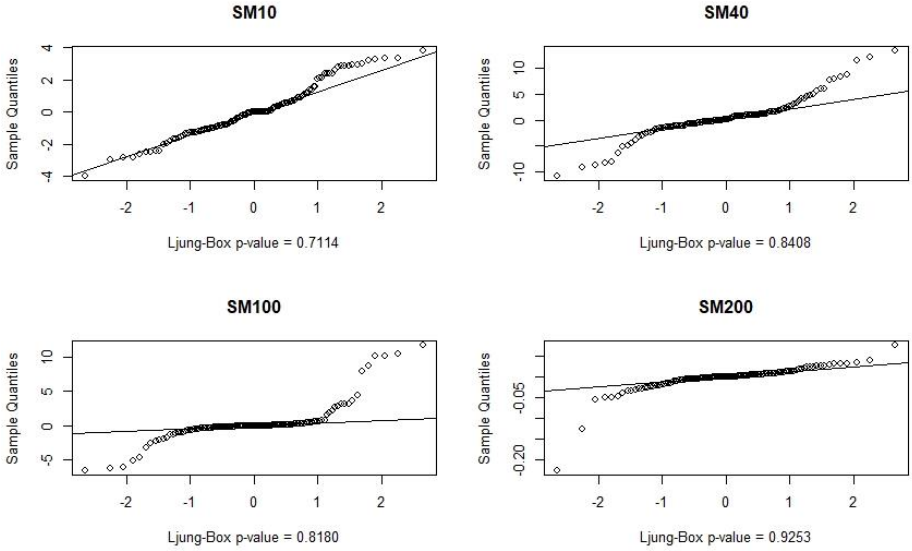



**Figure 4.** QQ plots of the predicted residuals of the seasonal ARIMA model at different depths.

Most of the residuals in Figure 4 closely follow the median trend line. And the Ljung-Box test has a p-value greater than 0.05, none of which rejects the original hypothesis. These indicate that the residuals meet the normality assumption and pass the white noise test, then the model can be considered to have adequately fitted the data and can be used in the next step of the forecasting process. The final predicted data were obtained as shown in Table 8.

**Table 8.** Predicted values of soil moisture based on seasonal ARIMA model.

| Year | Month | 10cm SM | 40cm SM | 100cm SM | 200cm SM |
|---|---|---|---|---|---|
| 2022 | 4 | 14.92 | 50.85 | 93.41 | 164.43 |
| | 5 | 15.94 | 49.00 | 93.41 | 164.34 |
| | 6 | 17.48 | 49.40 | 93.41 | 164.11 |
| | 7 | 19.81 | 58.23 | 93.41 | 163.85 |
| | 8 | 18.51 | 55.37 | 93.41 | 163.54 |

| | | | | | |
|---|---|---|---|---|---|
| 2023 | 9 | 17.64 | 56.20 | 93.41 | 163.23 |
| | 10 | 15.71 | 53.16 | 93.41 | 162.94 |
| | 11 | 14.00 | 51.28 | 93.41 | 162.78 |
| | 12 | 13.34 | 50.99 | 93.41 | 162.72 |
| | 1 | 12.60 | 50.81 | 93.41 | 162.69 |
| | 2 | 11.98 | 50.68 | 93.41 | 162.64 |
| | 3 | 12.73 | 50.57 | 93.41 | 162.57 |
| | 4 | 13.62 | 49.84 | 93.41 | 162.45 |
| | 5 | 15.18 | 48.55 | 93.41 | 162.32 |
| | 6 | 17.03 | 48.63 | 93.41 | 162.02 |
| | 7 | 19.54 | 55.45 | 93.41 | 161.69 |
| | 8 | 18.36 | 52.96 | 93.41 | 161.32 |
| | 9 | 17.55 | 54.00 | 93.41 | 160.97 |
| | 10 | 15.66 | 51.72 | 93.41 | 160.66 |
| | 11 | 13.97 | 50.32 | 93.41 | 160.50 |
| | 12 | 13.32 | 50.18 | 93.41 | 160.41 |

Soil moisture predictions based on the seasonal ARIMA model were obtained by combining the predicted data with the original data, while 95% confidence intervals were plotted for the predicted data, as shown in Figure 5.

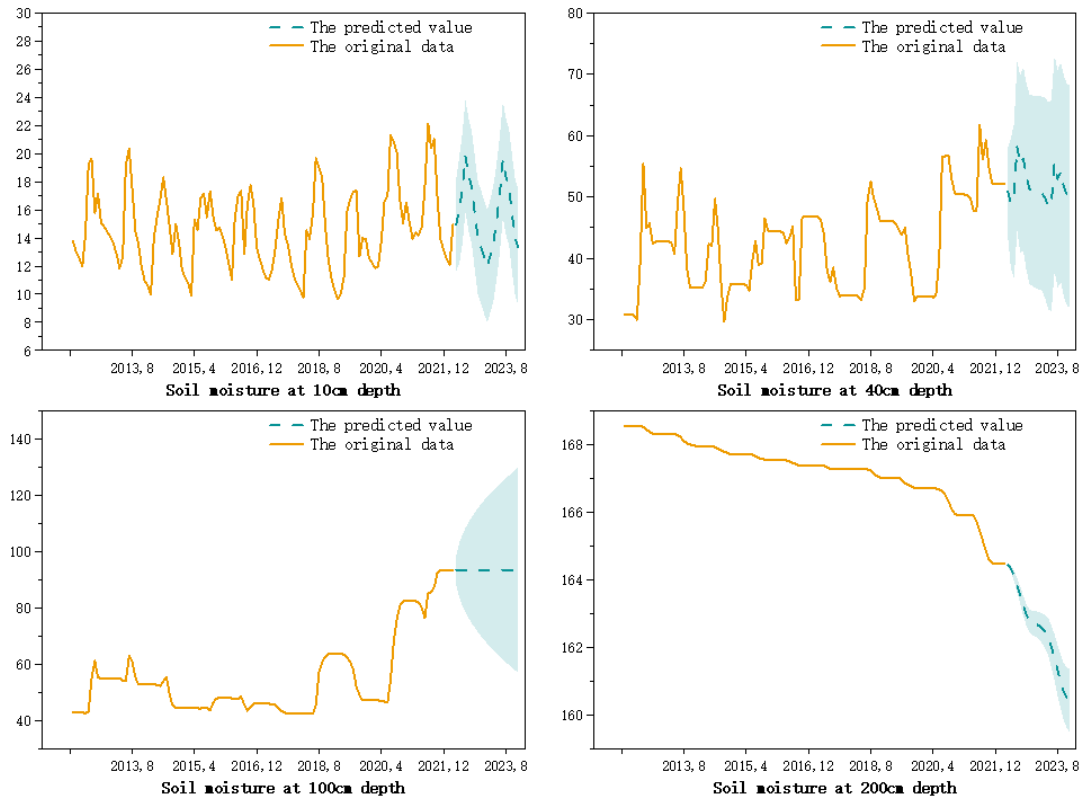



**Figure 5.** Soil moisture prediction results based on seasonal ARIMA model with 95% confidence interval.

From Figure 5, it can be seen that the predicted values and confidence intervals of soil moisture at 10 cm depth and 40 cm depth showed periodic fluctuations, but the confidence intervals were larger at 40 cm depth. At 100 cm, the model predicted a horizontal straight line with a significant increase in uncertainty and a flared spread of confidence

intervals. By 200 cm depth, the variation in soil moisture was smaller and the confidence intervals were not significant.

### *3.2. Model Comparison*

In order to see the trend of the prediction results more clearly, a comparison chart of the prediction trend is drawn, as shown in Figure 6. Model A represents the soil moisture prediction model based on depth and water balance equation, and Model B represents the soil moisture prediction model based on seasonal ARIMA model.

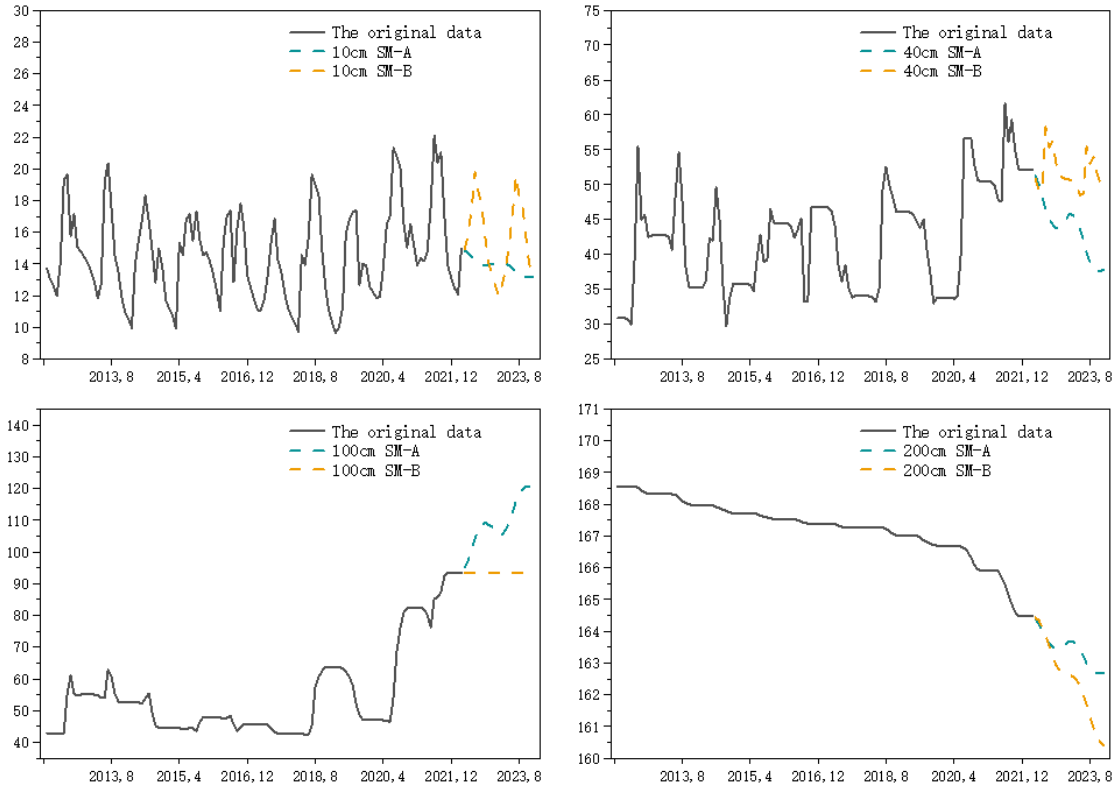



**Figure 6.** Comparison of the overall trend of soil moisture prediction by different models.

The predicted data and known data were combined to draw a line graph as shown in Figure 6. It can be seen from the Figure 6 that the prediction results of model A show a fluctuating decreasing trend at 10 cm, 40 cm and 200 cm, and at 100 cm the prediction value increases with the previous trend, while model B shows a different change. At a depth of 10 cm, model A predicts a gentle decline in soil moisture with time and a small range of variation, while model B predicts a cyclical fluctuating trend in soil moisture with large fluctuations, more in line with the previous trend. At a depth of 40 cm, model A predicts a fluctuating decline in soil moisture with time, but with large fluctuations, while model B predicts that soil moisture fluctuates back and forth within an interval with small changes. At a depth of 100 cm, model A predicts that soil moisture will continue to fluctuate upward with the previous trend, while model B predicts that soil moisture will remain constant. At a depth of 200 cm, model A predicts a small fluctuating decrease in soil moisture, while model B predicts a much larger fluctuating decrease in soil moisture. On the whole, the soil moisture showed a regular pattern of periodic changes involving large fluctuations, which is consistent with Cai's findings[36]. Model A showed a more moderate fluctuation at 10 cm and 200 cm, rising at 100 cm according to the previous trend, and fluctuating downward at other depths. Model B showed a clear cyclical pattern at 10 cm and 40 cm, predicted to remain constant at 100 cm, and declined more at 200 cm.

Using the data from January 2012 to December 2020 as the training set and January 2021 to March 2022 as the test set, the prediction errors of model A and model B were obtained, as shown in Table 9.

**Table 9.** Comparison of soil moisture prediction errors of different models.

| | 10cm SM | | 40cm SM | | 100cm SM | | 200cm SM | |
|---|---|---|---|---|---|---|---|---|
| | A | B | A | B | A | B | A | B |
| RMSE | 3.112 | **2.138** | **9.342** | 10.072 | **5.848** | 6.981 | **0.298** | 0.739 |
| MSE | 9.684 | **4.571** | **87.265** | 101.437 | **34.197** | 48.729 | **0.089** | 0.547 |
| MAE | 2.684 | **1.603** | **7.145** | 9.379 | **4.633** | 5.584 | **0.238** | 0.578 |
| MAPE | 16.629 | **9.299** | **12.951** | 17.529 | **5.411** | 6.207 | **0.144** | 0.351 |

*Note: The values marked in **bold** are the smaller error values at the same depth.

It is clear from Table 9 that, as a whole, the prediction errors of both models increase and then decrease with increasing depth, with the largest prediction error at 40 cm and the smallest prediction error at 200 cm. This may be due to the regularity of other influencing factors close to the surface, which creates a strong cycle. As the depth increases, the soil moisture is less affected by external influences until 200 cm when it basically maintains a stable state, so the prediction error at 200 cm is the smallest.

The error of model A is larger than model B at 10 cm because the soil at 10 cm is affected by the atmosphere, vegetation and other factors[37,38], creating a stronger periodicity that fluctuates within a smaller range, thus making the time series prediction method more accurate. However, with the increase of depth, the influence of uncertainties becomes larger and the advantage of model A comes into play. The errors of model A were smaller than model B at 40 cm, 100 cm and 200 cm depths, and model A has high accuracy in predicting soil moisture with weaker periodicity and regularity.

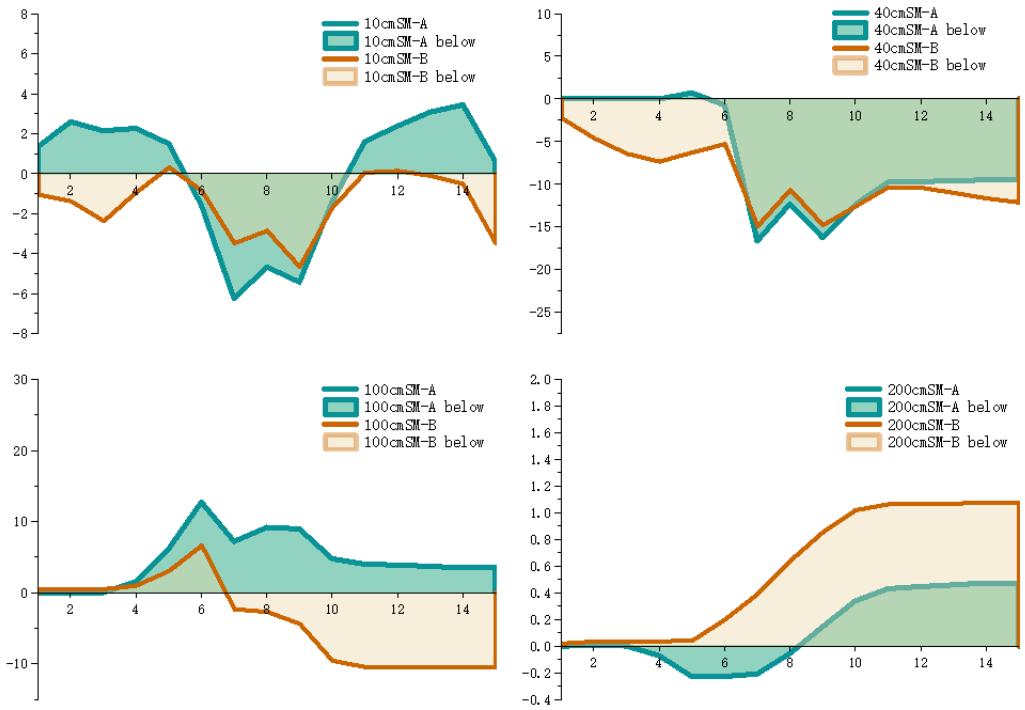



**Figure 7.** Predicted residual area maps of different models at different depths.

The prediction residuals for different depths are plotted as area plots, as shown in Figure 7. From Figure 7, it can be seen that the error fluctuation of model A at 10 cm is

slightly larger than that of model B, resulting in a lower overall prediction accuracy at 10 cm than that of model B. However, the prediction residuals of model A at 40 cm, 100 cm and 200 cm are smaller than that of model B, with smaller prediction errors and higher prediction accuracy.

The prediction of model B was better at 10 cm; the prediction of model A was better at 40 cm, 100 cm and 200 cm. This demonstrates the effectiveness of the soil moisture prediction model based on depth and water balance equation, which exhibits satisfactory prediction performance and prediction accuracy. More importantly, in soil moisture prediction, more accurate prediction values can be obtained using different methods. In this study, for example, a soil moisture prediction model based on the seasonal ARIMA model can be used at 10 cm, and a soil moisture prediction model based on depth and water balance equations can be used at 40 cm, 100 cm and 200 cm.

In summary, this study proposes a soil moisture prediction model based on depth and water balance equation that combines water balance equation and seasonal ARIMA model. Compared to predicting soil moisture using methods such as machine learning[39–41], the model can explain the variables and model principles with theoretical significance. Compared to the monitoring and prediction of soil moisture using remote sensing data[42–44], the model is not only able to predict soil moisture at the surface, but also at different depths based on the inclusion of depth coefficients. The experimental results showed that the model proposed in this study was able to provide higher prediction accuracy for soil moisture prediction at 40 cm, 100 cm and 200 cm compared to the soil moisture prediction model based on seasonal ARIMA model. The RMSEs of the model were 3.112, 9.342, 5.848 and 0.298 at 10 cm, 40 cm, 100 cm and 200 cm, respectively, and the overall predicted values were close to the true values, which could accurately predict soil moisture.

## 4. Conclusions

### *4.1. Theoretical Contributions*

Soil moisture plays a key role in the sustainability of grasslands, as predicting soil moisture helps to improve drought prediction and agricultural crop production, leading to appropriate irrigation, grazing plans and water management. The physics-based process model is more complex, and the absence or lack of information can introduce some errors into soil moisture prediction. Since the equations are built on the assumption of independence of local laws, they are not suitable for medium to long term predictions. Data-driven empirical models, such as machine learning, are questionable because the principles of prediction are not available, and too little data can lead to underfitting and other problems. To address these shortcomings, this study proposes a novel hybrid model for predicting soil moisture, a soil moisture prediction model based on depth and water balance equation, which integrates the water balance equation with seasonal ARIMA model and introduces a depth parameter to predict soil moisture at different depths. The model has a high prediction accuracy at 40 cm, 100 cm and 200 cm. This study also proposes that different models can be used for prediction at different depths, for example, using the soil moisture prediction model based on seasonal ARIMA model at 10 cm and the soil moisture prediction model based on depth and water balance equation at 40 cm, 100 cm and 200 cm, from which more accurate prediction values can be obtained.

### *4.2. Policy Implications*

At present, due to population growth and economic development, the intensity of land use has been increasing, leading to a broken ecological environment of land resources and the emergence of more and more fragile ecological areas. This seriously threatens the ecological security of regional land resources and directly affects the sustainable development of the region. The scientific evaluation of the ecological safety of regional land resources and the rational use of land are related to the fate of the country and social development. Soil moisture plays an important role in the research and application of climate,

environment and ecology, which can well reflect the ecological environment quality status of the region and is an important indicator for monitoring the surface environment. Accurate prediction of soil moisture can provide an important theoretical basis for sustainable land use, water resources planning and management, and agricultural production. This has important implications for regional ecosystem conservation.

Different types of soils require different policies to protect regional ecosystems. In this study, the Xilingol League grassland is used as an example. The prediction shows that by December 2023, the soil moisture at 10cm will show a strong periodic fluctuation as before, the soil moisture at 40cm and 200cm will fluctuate down, and the soil moisture at 100cm will maintain the previous trend of rising. Overall, the moisture at 40 cm, 100 cm and 200 cm is roughly 3.88, 6.67 and 13.51 times that of the moisture at 10 cm. The Xilingol League grassland in Inner Mongolia has low precipitation and uneven distribution, and in the process of promoting its sustainable development, ecological protection should be the center, and some local areas with severely degraded grasslands should be the priority areas for construction and protection work. In order to prevent the increase of soil aridity and thus prevent land desertification and soil slabbing, appropriate irrigation plans can be made and appropriate grazing can be achieved to realize scientific management of grasslands[45]. This promotes the ecological stability and the sustainable development of grassland while rationalizing land use.

### *4.3. Limitations*

Soil moisture is a complex nonlinear coupled system, which is greatly influenced by the external environment and other factors. The limitations of this study mainly exist in the following two points. First, the nature of different soils is different. This study was done only for grasslands in the Xilingol League, and there is a lack of research on soil moisture relationships in other types of soils. Second, in order to simplify the study, more assumptions were set in this study, which may be different from the real situation.

### *4.4. Future Research Perspectives*

In view of the shortcomings of the research in this paper, the paper can be improved in the following two aspects when the conditions allow. First, different soils are classified, exclusive models are constructed for different types of soils, and professional policies are provided according to regional conditions. Second, soil moisture is influenced by more external factors, and since the parameters are related to fixed-point data, the association between local factors can be studied in depth, and the association between soil moisture and its influencing factors in different regions can also be explored. Thus, the constraint assumptions can be released as much as possible to improve the generalization ability of the model and form a model that can be further promoted. Subsequent research can be conducted based on the above two aspects to obtain more accurate soil moisture prediction values, which can then promote sustainable land use and sustainable development of regional ecology.

**Author Contributions:** Conceptualization, R.F. and L.X.; methodology, R.F.; software, L.X.; validation, B.Z. and R.F.; formal analysis, T.L. and Y.Z.; investigation, Y.Z.; resources, R.F.; data curation, L.X. and S.H.; writing—original draft preparation, L.X.; writing—review and editing, R.F.; visualization, B.Z.; supervision, S.H.; project administration, T.L.; funding acquisition, R.F. All authors have read and agreed to the published version of the manuscript.

**Funding:** This research was funded by the National Social Science Foundation (Grant No.20BTJ005).

**Institutional Review Board Statement:** Not applicable.

**Informed Consent Statement:** Not applicable.

**Data Availability Statement:** Data sources are contained within the article.

**Acknowledgments:** We would like to thank the reviewers for their valuable comments and efforts.

**Conflicts of Interest:** The authors declare no conflict of interest.

## References


1. Huang, S.; Ding, J.; Zou, J.; Liu, B.; Zhang, J.; Chen, W. Soil Moisture Retrival Based on Sentinel-1 Imagery under Sparse Vegetation Coverage. *Sensors* **2019**, *19* (3), 589. https://doi.org/10.3390/s19030589.
2. Haregeweyn, N.; Tesfaye, S.; Tsunekawa, A.; Tsubo, M.; Meshesha, D. T.; Adgo, E.; Elias, A. Dynamics of Land Use and Land Cover and Its Effects on Hydrologic Responses: Case Study of the Gilgel Tekeze Catchment in the Highlands of Northern Ethiopia. *Environ Monit Assess* **2015**, *187* (1), 4090. https://doi.org/10.1007/s10661-014-4090-1.
3. Walker, J. P.; Willgoose, G. R.; Kalma, J. D. One-Dimensional Soil Moisture Profile Retrieval by Assimilation of Near-Surface Measurements: A Simplified Soil Moisture Model and Field Application. *J. Hydrometeor* **2001**, *2* (4), 356–373. https://doi.org/10.1016/S0309-1708(00)00043-9.
4. Yu, L.; Gao, W.; R. Shamshiri, R.; Tao, S.; Ren, Y.; Zhang, Y.; Su, G. Review of Research Progress on Soil Moisture Sensor Technology. *International Journal of Agricultural and Biological Engineering* **2021**, *14* (3), 32–42. https://doi.org/10.25165/j.ijabe.20211404.6404.
5. Schulte, R. P. O.; Diamond, J.; Finkele, K.; Holden, N. M.; Brereton, A. J. Predicting the Soil Moisture Conditions of Irish Grasslands. *Irish Journal of Agricultural and Food Research* **2005**, *44* (1), 95–110. https://doi.org/10.2307/25562535.
6. Seneviratne, S. I.; Corti, T.; Davin, E. L.; Hirschi, M.; Jaeger, E. B.; Lehner, I.; Orlowsky, B.; Teuling, A. J. Investigating Soil Moisture–Climate Interactions in a Changing Climate: A Review. *Earth-Science Reviews* **2010**, *99* (3–4), 125–161. https://doi.org/10.1016/j.earscirev.2010.02.004.
7. Wang, C.; Fu, B.; Zhang, L.; Xu, Z. Soil Moisture–Plant Interactions: An Ecohydrological Review. *J Soils Sediments* **2019**, *19* (1), 1–9. https://doi.org/10.1007/s11368-018-2167-0.
8. Mohammadi, B. Application of Machine Learning and Remote Sensing in Hydrology. *Sustainability* **2022**, *14* (13), 7586. https://doi.org/10.3390/su14137586.
9. Luo, D.; Wen, X.; Xu, J. All-Sky Soil Moisture Estimation over Agriculture Areas from the Full Polarimetric SAR GF-3 Data. *Sustainability* **2022**, *14* (17), 10866. https://doi.org/10.3390/su141710866.
10. Duerinck, H. M.; van der Ent, R. J.; van de Giesen, N. C.; Schoups, G.; Babovic, V.; Yeh, P. J.-F. Observed Soil Moisture–Precipitation Feedback in Illinois: A Systematic Analysis over Different Scales. *Journal of Hydrometeorology* **2016**, *17* (6), 1645–1660. https://doi.org/10.1175/JHM-D-15-0032.1.
11. Li, Z.; Zhou, T.; Chen, H.; Ni, D.; Zhang, R. Modelling the Effect of Soil Moisture Variability on Summer Precipitation Variability over East Asia. *Int. J. Climatol.* **2015**, *35* (6), 879–887. https://doi.org/10.1002/joc.4023.
12. Dirmeyer, P. A.; Gao, X.; Zhao, M.; Guo, Z.; Oki, T.; Hanasaki, N. GSWP-2: Multimodel Analysis and Implications for Our Perception of the Land Surface. *Bulletin of the American Meteorological Society* **2006**, *87* (10), 1381–1398. https://doi.org/10.1175/BAMS-87-10-1381.
13. Rosenbaum, U.; Bogena, H. R.; Herbst, M.; Huisman, J. A.; Peterson, T. J.; Weuthen, A.; Western, A. W.; Vereecken, H. Seasonal and Event Dynamics of Spatial Soil Moisture Patterns at the Small Catchment Scale. *Water Resour. Res.* **2012**, *48* (10), 2011WR011518. https://doi.org/10.1029/2011WR011518.
14. Short Gianotti, D. J.; Akbar, R.; Feldman, A. F.; Salvucci, G. D.; Entekhabi, D. Terrestrial Evaporation and Moisture Drainage in a Warmer Climate. *Geophys. Res. Lett.* **2020**, *47* (5). https://doi.org/10.1029/2019GL086498.
15. Chen, M.; Willgoose, G. R.; Saco, P. M. Spatial Prediction of Temporal Soil Moisture Dynamics Using HYDRUS-1D: HYDRUS-1D SOIL MOISTURE MODEL. *Hydrol. Process.* **2014**, *28* (2), 171–185. https://doi.org/10.1002/hyp.9518.
16. Traff, D. C.; Niemann, J. D.; Middlekauff, S. A.; Lehman, B. M. Effects of Woody Vegetation on Shallow Soil Moisture at a Semiarid Montane Catchment: EFFECTS OF WOODY VEGETATION ON SHALLOW SOIL MOISTURE. *Ecohydrol.* **2015**, *8* (5), 935–947. https://doi.org/10.1002/eco.1542.
17. Zhu, S.; Chen, H.; Dong, X.; Wei, J. Influence of Persistence and Oceanic Forcing on Global Soil Moisture Predictability. *Clim Dyn* **2020**, *54* (7–8), 3375–3385. https://doi.org/10.1007/s00382-020-05184-8.
18. Mo, K. C.; Lettenmaier, D. P. Hydrologic Prediction over the Conterminous United States Using the National Multi-Model Ensemble. *Journal of Hydrometeorology* **2014**, *15* (4), 1457–1472. https://doi.org/10.1175/JHM-D-13-0197.1.
19. Huang, S.; Huang, Q.; Leng, G.; Zhao, M.; Meng, E. Variations in Annual Water-Energy Balance and Their Correlations with Vegetation and Soil Moisture Dynamics: A Case Study in the Wei River Basin, China. *Journal of Hydrology* **2017**, *546*, 515–525. https://doi.org/10.1016/j.jhydrol.2016.12.060.
20. Tang, L.; Zhang, Y.; Shi, H.; Hu, Y. Runoff Generation, Confluence Mechanism, and Water Balance Change of Coal Mining Areas with Goaf: Establishment of a Runoff Prediction Model. *Journal of Hydrology* **2021**, *603*, 127023. https://doi.org/10.1016/j.jhydrol.2021.127023.
21. Mei, X.; Ma, L.; Zhu, Q.; Li, B.; Zhang, D.; Liu, H.; Zhang, Q.; Gou, Q.; Shen, M. The Variability in Soil Water Storage on the Loess Hillslopes in China and Its Estimation. *CATENA* **2019**, *172*, 807–818. https://doi.org/10.1016/j.catena.2018.09.045.
22. Qiu, Y.; Fu, B.; Wang, J.; Chen, L. Spatiotemporal Prediction of Soil Moisture Content Using Multiple-Linear Regression in a Small Catchment of the Loess Plateau, China. *CATENA* **2003**, *54* (1–2), 173–195. https://doi.org/10.1016/S0341-8162(03)00064-X.
23. Kim, J.; Mohanty, B. P.; Shin, Y. Effective Soil Moisture Estimate and Its Uncertainty Using Multimodel Simulation Based on Bayesian Model Averaging. *JGR Atmospheres* **2015**, *120* (16), 8023–8042. https://doi.org/10.1002/2014JD022905.

24. Ganguli, P.; Reddy, M. J. Ensemble Prediction of Regional Droughts Using Climate Inputs and the SVM-Copula Approach: ENSEMBLE PREDICTION OF REGIONAL DROUGHTS. *Hydrol. Process.* **2014**, *28* (19), 4989–5009. https://doi.org/10.1002/hyp.9966.
25. Liu, D.; Mishra, A. K.; Yu, Z. Evaluating Uncertainties in Multi-Layer Soil Moisture Estimation with Support Vector Machines and Ensemble Kalman Filtering. *Journal of Hydrology* **2016**, *538*, 243–255. https://doi.org/10.1016/j.jhydrol.2016.04.021.
26. Bonakdari, H.; Moeeni, H.; Ebtehaj, I.; Zeynoddin, M.; Mahoammadian, A.; Gharabaghi, B. New Insights into Soil Temperature Time Series Modeling: Linear or Nonlinear? *Theor Appl Climatol* **2019**, *135* (3–4), 1157–1177. https://doi.org/10.1007/s00704-018-2436-2.
27. Jung, C.; Lee, Y.; Cho, Y.; Kim, S. A Study of Spatial Soil Moisture Estimation Using a Multiple Linear Regression Model and MODIS Land Surface Temperature Data Corrected by Conditional Merging. *Remote Sensing* **2017**, *9* (8), 870. https://doi.org/10.3390/rs9080870.
28. Nguyen, T. T. A Low-Cost Approach for Soil Moisture Prediction Using Multi-Sensor Data and Machine Learning Algorithm. *Science of the Total Environment* **2022**, 12. https://doi.org/10.1016/j.scitotenv.2022.155066.
29. Hegazi, E. H.; Yang, L.; Huang, J. A Convolutional Neural Network Algorithm for Soil Moisture Prediction from Sentinel-1 SAR Images. *Remote Sensing* **2021**, *13* (24), 4964. https://doi.org/10.3390/rs13244964.
30. Liu, D.; Liu, C.; Tang, Y.; Gong, C. A GA-BP Neural Network Regression Model for Predicting Soil Moisture in Slope Ecological Protection. *Sustainability* **2022**, *14* (3), 1386. https://doi.org/10.3390/su14031386.
31. Chen, M.; Willgoose, G. R.; Saco, P. M. Investigating the Impact of Leaf Area Index Temporal Variability on Soil Moisture Predictions Using Remote Sensing Vegetation Data. *Journal of Hydrology* **2015**, *522*, 274–284. https://doi.org/10.1016/j.jhydrol.2014.12.027.
32. Cui, Y.; Zhao, P.; Yan, B.; Xie, H.; Yu, P.; Wan, W.; Fan, W.; Hong, Y. Developing the Remote Sensing-Gash Analytical Model for Estimating Vegetation Rainfall Interception at Very High Resolution: A Case Study in the Heihe River Basin. *Remote Sensing* **2017**, *9* (7), 661. https://doi.org/10.3390/rs9070661.
33. Hou, Q.; Wang, Y.; Yang, Z.; Shi, G. Soil Water Dynamics Model of Typical Grassland in Inner Mongolia Based on Water Balance Principle. *Agricultural Research in the Arid Areas* **2011**, *29* (05), 197–203. https://doi.org/61-1088/S.
34. Hyndman, R. J.; Khandakar, Y. Automatic Time Series Forecasting: The Forecast Package for R. *J. Stat. Soft.* **2008**, *27* (3). https://doi.org/10.18637/jss.v027.i03.
35. Glenn, E.; Huete, A.; Nagler, P.; Nelson, S. Relationship Between Remotely-Sensed Vegetation Indices, Canopy Attributes and Plant Physiological Processes: What Vegetation Indices Can and Cannot Tell Us About the Landscape. *Sensors* **2008**, *8* (4), 2136–2160. https://doi.org/10.3390/s8042136.
36. Cai, Y.; Zheng, W.; Zhang, X.; Zhangzhong, L.; Xue, X. Research on Soil Moisture Prediction Model Based on Deep Learning. *PLoS ONE* **2019**, *14* (4), e0214508. https://doi.org/10.1371/journal.pone.0214508.
37. Alavi, N.; Bélair, S.; Fortin, V.; Zhang, S.; Husain, S. Z.; Carrera, M. L.; Abrahamowicz, M. Warm Season Evaluation of Soil Moisture Prediction in the Soil, Vegetation, and Snow (SVS) Scheme. *Journal of Hydrometeorology* **2016**, *17* (8), 2315–2332. https://doi.org/10.1175/JHM-D-15-0189.1.
38. Almendra-Martín, L.; Martínez-Fernández, J.; Piles, M.; González-Zamora, Á.; Benito-Verdugo, P.; Gaona, J. Influence of Atmospheric Patterns on Soil Moisture Dynamics in Europe. *Science of The Total Environment* **2022**, *846*, 157537. https://doi.org/10.1016/j.scitotenv.2022.157537.
39. Chatterjee, S.; Dey, N.; Sen, S. Soil Moisture Quantity Prediction Using Optimized Neural Supported Model for Sustainable Agricultural Applications. *Sustainable Computing: Informatics and Systems* **2020**, *28*, 100279. https://doi.org/10.1016/j.suscom.2018.09.002.
40. Jiang, S.; Chen, G.; Chen, D.; Chen, T. Application and Evaluation of an Improved LSTM Model in the Soil Moisture Prediction of Southeast Chinese Tobacco-Producing Areas. *J Indian Soc Remote Sens* **2022**. https://doi.org/10.1007/s12524-021-01438-y.
41. Li, Q.; Wang, Z.; Shangguan, W.; Li, L.; Yao, Y.; Yu, F. Improved Daily SMAP Satellite Soil Moisture Prediction over China Using Deep Learning Model with Transfer Learning. *Journal of Hydrology* **2021**, *600*, 126698. https://doi.org/10.1016/j.jhydrol.2021.126698.
42. Montaldo, N.; Fois, L.; Corona, R. Soil Moisture Estimates in a Grass Field Using Sentinel-1 Radar Data and an Assimilation Approach. *Remote Sensing* **2021**, *13* (16), 3293. https://doi.org/10.3390/rs13163293.
43. Montaldo, N.; Gaspa, A.; Corona, R. Multiscale Assimilation of Sentinel and Landsat Data for Soil Moisture and Leaf Area Index Predictions Using an Ensemble-Kalman-Filter-Based Assimilation Approach in a Heterogeneous Ecosystem. *Remote Sensing* **2022**, *14* (14), 3458. https://doi.org/10.3390/rs14143458.
44. Urban, M.; Berger, C.; Mudau, T. E.; Heckel, K.; Truckenbrodt, J.; Odipo, V. O.; Smit, I. P. J.; Schmullius, C. Surface Moisture and Vegetation Cover Analysis for Drought Monitoring in the Southern Kruger National Park Using Sentinel-1, Sentinel-2, and Landsat-8. *Remote Sensing* **2018**, *10* (9), 1482. https://doi.org/10.3390/rs10091482.
45. Tian, Y.; Liu, Y.; Jin, J. Effect of Irrigation Schemes on Forage Yield, Water Use Efficiency, and Nutrients in Artificial Grassland under Arid Conditions. *Sustainability* **2017**, *9* (11), 2035. https://doi.org/10.3390/su9112035.